Phase and Mixing Behavior in Two-Component Lipid Bilayers: A Molecular Dynamics Study in DLPC/DSPC Mixtures

Sandra V. Bennun, Margie Longo, and Roland Faller*

Department of Chemical Engineering and Materials Science, University of California−Davis, California 95616

Received: March 15, 2007; In Final Form: June 1, 2007

Phase and mixing behavior of dilauroylphosphatidylcholine (DLPC)/distearoylphosphatidylcholine (DSPC) lipid mixtures are studied by molecular dynamics simulations with use of a coarse-grained model over a wide range of concentrations. The results reveal that phase transformations from the fluid to the gel state can be followed over a microsecond time scale. The changes in structure suggest regions of phase coexistence allowing us to outline the entire phase diagram for this lipid mixture using a molecular based model. We show that simulations yield good agreement with the experimental phase diagram. We also address the effect of macroscopic phase separation on the determination of the transition temperature, different leaflet composition, and finite size effects. This study may have implications on lateral membrane organization and the associated processes dependent on these membrane regions on different time and length scales.

1. Introduction

Heterogeneities in cell membranes[1−6] associated with lipids of different degree of order have led to fundamental questions about the functionality and role of the phase behavior of the lipids in membrane processes. An important characteristic of real cell membranes is the unequal concentrations in the two leaflets. Several approaches have been directed toward achieving nanometer resolution in order to understand local-scale phase behavior.[7−10] The study of lipid mixtures with the aim to reveal the basis of the complex mixing and phase behavior of the lipids in cell membranes has gained a lot of attention. In real cell membranes it is nearly impossible to obtain a clear picture because of the complex lipid composition, the presence of proteins, and other cell constituents.[11−13] Therefore most studies have focused on model lipid mixtures to understand complex systems.[14−17] Lipid phase diagrams play an important role for understanding the interactions in lipid mixtures and for interpreting the role of these interactions in the cell membrane.[18−21] Few theoretical studies have been able to capture the dynamics of the thermotropic phase transformation at the nanometer scale.[8−10,22,23] The dynamics of the thermotropic behavior of a lipid mixture over the whole range of compositions to generate a phase diagram has not been approached yet by a molecular based model. The reasons are the large size and time scales needed to obtain phase separation, which are not within reach of atomistic molecular dynamics simulations. Monte Carlo simulation methods using simple models have therefore been mostly used to study phase behavior of lipid mixtures.[15,16] However Monte Carlo does not offer time scales. Here we describe a systematic study of the properties of mixed dilauroylphosphatidylcholine (DLPC)/distearoylphosphatidylcholine (DSPC) bilayers using a well-tested coarse-grained molecular model.[24] An important aspect of this model is that a coarse-grained lipid resembles and maintains the fundamental chemical and physical nature of a specific lipid molecule. This model has been used to reproduce accurate values of experimentally measured properties for lipids in the liquid crystalline and gel phase;[24] we use it without any further modification. All parameters can be found in ref 24. Vesicle fusion and formation,[25] as well as hexagonal phase formation,[26] have been captured at the molecular level, and the phase behavior of lipids has also been semiquantitatively reproduced.[8,9,22]

The lipids in our bilayers are saturated phosphatidylcholines differing only in the length of their tails. DSPC contains 18 carbons in both tails and its main transition temperature is 328 K.[18] DLPC has 12 carbons and a transition temperature of 268 K.[18] Thus, there is a sizable region of possible phase coexistence between a fluid or liquid crystalline state and a gel state. At room temperature DLPC is in the liquid crystalline state, and in this state lipids show weak interlipid van der Waals interactions with diffusion coefficients on the order of 10^{-7} cm^2/s,[27] indicating fast lateral diffusion at biologically relevant scales. DSPC lipids at room temperature are in the gel phase, where their low diffusion coefficients result from the lipids presenting stronger interlipid van der Waals interactions that preserve a lateral packing structure in the lattice; diffusion coefficients for this state are on the order of $\sim 10^{-9}$ cm^2/s. The DLPC/DSPC two-component phase diagram was determined experimentally by differential scanning calorimetry.[18] Theoretical approaches have also investigated this system. For instance, a phase diagram was constructed by using regular solution theory[19] and a statistical thermodynamic model, where essential parameters were adjusted to agree with the experimental data.[28] One of the main obstacles to study the phase behavior of this system from experiment or theory is the intervening freezing of water before DLPC transitions into the gel phase. Also the sensitivity to thermal history makes phase behavior studies problematic. So it is not surprising that there are no studies of the dynamic thermotropic behavior of any lipid mixture over the whole composition range to generate a phase diagram using a molecular based model.

Our approach differs from previous ones in that we can capture molecular detailed interactions over time in order to understand the dynamics of the lipids and to assess the lateral distributions of the components at the super atom level (i.e.,

* Address correspondence to this author. Phone: 530-752-5839. E-mail: rfaller@ucdavis.edu.

10.1021/jp072101q CCC: $37.00
Published on Web 07/17/2007

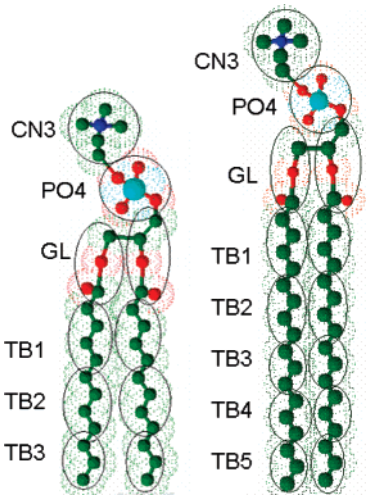

Figure 1. Representation of coarse-grained DLPC-DSPC. Each bead is composed of 4−6 atoms.

coarse-grained interaction site). We study the dynamics of mixing in a wide range of molar ratios of DLPC and DSPC on the time scales of microseconds and present an outline of a phase diagram of a lipid mixture of DLPC and DSPC. We discuss the feasibility of outlining a phase diagram by molecular dynamics and present the data that support and conflict with this model and approach. The study of such a two-component lipid mixture may contribute to the understanding of the phase behavior of complex lipid mixtures on the nanometer scale.

2. Simulation Model and Technique

Phospholipid mixtures of various molar ratios (1:4; 1:3; 1:1; 4:1; 3:1) of DLPC:DSPC mixtures as well as pure DLPC and DSPC are simulated by using a coarse-grained Molecular Dynamics model[24] at different temperatures. In this coarse-grained model groups of 4 to 6 heavy atoms are represented by one bead or superatom; this approach allows reaching relevant times and length scales.[8,9,22,23,29] Figure 1 shows the coarse-grained representations of DLPC and DSPC. DLPC consists of 10 interaction sites (beads), while DSPC consists of 14 interaction sites. One polar coarse-grained water bead represents 4 real water molecules. We use here the terminology "polar" to describe a force-field parameter representing a polar unit. The water force-field itself, however, does not use polar interactions. All beads interact through short-range Lennard-Jones and reaction field electrostatic potentials. The interaction among particles is given by the hydrophilic and hydrophobic nature of the interaction sites which is represented by the level and the strength of the interaction. Choline and phosphate groups are hydrophilic, glycerol is of intermediate hydrophilicity, and the two tails of the lipids are modeled by 3 and 5 hydrophobic sites corresponding to DLPC and DSPC, respectively. All bead types have the same mass of 72 amu, which corresponds to 4 water molecules and a size of 0.47 nm. Charged beads interact via a reaction-field version of the Coulombic potential in addition to a shifted Lennard-Jones interaction. We use harmonic bonds with nonbonded interactions excluded between bonded particles. Chain stiffness of the lipids is represented by a weak cosine-harmonic potential. The GROMACS simulation suite[30] version 3.2 has been used to perform all simulations. In order to obtain the correct diffusivities, time scales have been renormalized by a factor of 4, and the reported simulation times are real times. This renormalization factor has been empirically determined but is common to all lipids as well as water.[9,24] Unless stated otherwise, simulations lasted for 4 μs with a time step of 160 fs, where we only used the last 3.6 μs for analysis, except for the diffusion analysis where the run was divided into several time intervals to provide better statistical data. Snapshots were stored every 1000 steps. Temperature and pressure are kept constant by using the weak-coupling method.[31] For pressure the coupling is applied to the three Cartesian directions independently.

Molecular dynamics simulations were performed in fully hydrated systems. The details of compositions, temperatures, and simulation times with their respective system sizes are given in Table 1. The pure lipid systems contain 200 DLPC or 200 DSPC lipids. The equimolar mixtures contain at least 512 lipids, and the 1:3, 1:4, 3:1, and 4:1 mixtures (all concentrations are molar) contain at least 256, or 320 lipids. We also performed simulations of larger bilayer systems for selected concentrations in order to evaluate finite size effects on the mixing and phase behavior. For the equimolar mixture and for the 1:3 DSPC−DLPC mixture bilayers containing 2048 lipids and for the 1:4 DSPC−DLPC molar composition a bilayer containing 2560 lipids were studied.

All bilayers were obtained by randomly distributing DLPC and DSPC in each leaflet in equal concentrations except where noted otherwise. Larger systems were constructed by multiplying smaller bilayers in x and y directions. All starting structures were in the liquid crystalline phase in order to erase possible memory of clustering; simulations were cooled by quenching from high temperature to the target temperature under NPT conditions. We also performed some simulations by heating in one step (inverse quenching) an equilibrated bilayer at low temperature to the desired higher temperature, and found that these lipid bilayers present a high level of hysteresis as reported experimentally[17] and by simulation.[8]

Pure water was also simulated in order to characterize the behavior for this coarse-grained water model. Note that the number of waters has to be rescaled by a factor of 4 (see above). Densities as a function of temperature curves were obtained by using cooling and heating cycles. We refer to the heating cycle as the process of increasing the simulation temperature gradually to a desired temperature after each run, in the same way in the cooling cycle the simulation temperature is decreased after each run. Systems with 1500 water molecules in box sizes ranging from $4 \times 5 \times 8$ nm^3 at 265 K to $4 \times 5.4 \times 8.5$ nm^3 at 325 K were simulated at constant temperature and pressure for 4 μs.

3. Results and Discussions

3.1. Coarse-Grained Water. As discussed above the freezing point of the water is crucial in the determination of the phase behavior of lipid mixtures since frozen water in the vicinity of a lipid bilayer may lead to unnatural phase behavior. We first evaluated the freezing point of the coarse-grained water by determining the inflection point in the density−temperature diagram for cooling and heating cycles as well as static structure factors. The changes of the structure with temperature correlate with the changes of density with the temperature for cooling and heating cycles.[32] We found that for systems of 1500 CG waters the freezing point for cooling cycles is between 260 and 275 K and for heating cycles between 325 and 385 K showing very strong hysteresis. Since most of our simulations were done in cooling cycles we can conclude that our coarse-grained water freezes at ~265 K under cooling (see the structure factor for the cooling cycle in Figure 2). We will show a transition temperature (T_m) for DLPC of 265 K. One may argue that this is biased by freezing of water before DLPC reaches its T_m.

TABLE 1: Composition, System Sizes, Temperatures, and Simulation Times[a]

composition				
water	DLPC	DSPC	system size X−Y−Z (nm)	temperature (K)
1500			4−5−8	250, 260, 265, 275, 285, 295, 325, 385 (heating cycle) 385, 325, 295, 285, 275, 265, 260, 250 (cooling cycle)
6000		200	7−7−21	280, 285, 290, 300, 305, 325, 345, 385 (cooling cycle) 385, 345, 325, 315, 305, 295 (heating cycle)
3750	256	64	8−12−9	265, 270, 272, 275, 280, 285, 295, 325, 385, 400
15000	1024	256	13−26−9$^{(275K)}$	275$^{(4us)}$
30000	2048	512	26−27−9$^{(275K)}$	270$^{(1543ns)}$, 275$^{(1423ns)}$, 325 $^{(469ns)}$, 400$^{(339ns)}$
3000	192	64	7−11−9	265, 270, 273, 275, 280, 285, 295, 325, 335, 385
	1036	512		273$^{(4us)}$
3750	256	256	11−13−9	265, 275, 280, 285, 295, 305, 325, 345, 365, 385
24000	1024	1024	23−28−9$^{(275K)}$	275$^{(2970\ ns)}$, 325$^{(1862ns)}$
3750	64	192	8−8−11	265, 275, 285, 295, 305, 325, 385
3750	64	256	10−8−10	265, 275, 285, 295, 305, 325, 385
3750	200		6−9−11	265, 275, 285, 295, 305, 325, 385

[a] The temperature at which system sizes are reported is 285 K unless indicated by the superscripts, values were rounded up and the error due to fluctuations was estimated in order of 2% to 4%.

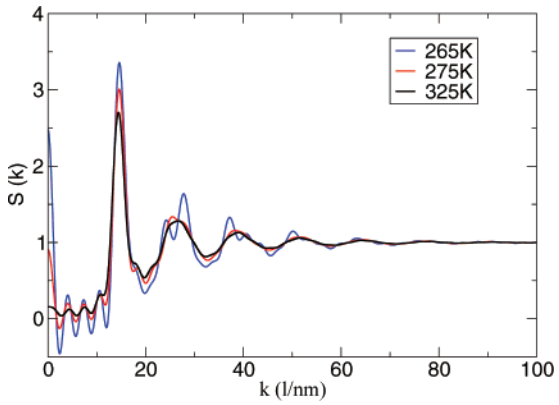

Figure 2. Coarse-grained water static structure factor for cooling cycles at different temperatures shows a clear change in the water structure from 275 to 265 K.

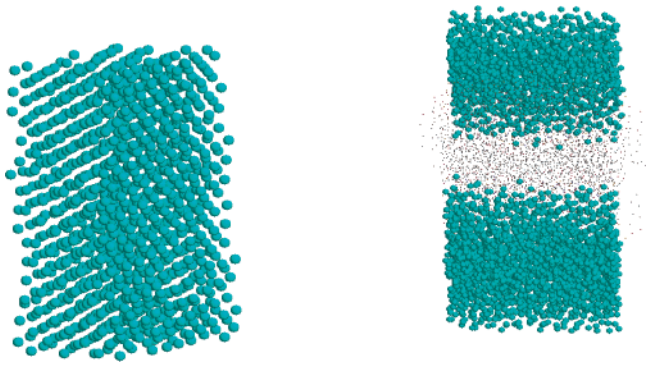

Figure 3. Water snapshots: On the left pure coarse-grained water at 265 K, presenting a crystalline structure, which correlates with water structure factor Figure 2. On the right side, coarse-grained water in contact with a DLPC bilayer at 265 K does not present a crystalline structure.

However, we find in our simulations for lipid bilayers in water at 265 K that the water structure surrounding the bilayer does not present a crystalline order compared with simulations of pure water at 265 K (cf. Figure 3). This may be attributed to two effects: the size effect, in our bilayer simulations we have always at least 4000 CG waters, and also the thermal history, since for the water in contact with the bilayers, the simulations were driven to the desired temperature without a ramp (i.e., the system was quenched), this effect may suppress water freezing. So we may have fluid supercooled water at temperatures below 270 K. A third reason may actually be the bilayer disturbing the water ordering. We did not explore the behavior of bilayers below 265 K since it is beyond the scope of this study.

3.2. Phase Transition in Lipid Mixtures. To investigate the main phase transition in the bilayer systems we determined the transition temperatures for the lipid mixtures. We evaluated the area per head group and the lipid (deuterium) order parameters as indicators of the lipid phase state. The area per head group is defined as the $x \times y$ box lengths (z is the bilayer normal) of the system divided by the number of lipids in a leaflet; our results are in agreement with experimentally measured liquid and gel phase areas.[33−35] For DLPC the simulated area is 0.58 nm^2 at 298 K and the experimental value is 0.57 nm^2 at 293 K.[35] DSPC presents an area of 0.64 nm^2 at 325 K, while its experimental value is 0.65 nm^2 at 333 K.[35] Abrupt changes in the area per head group from typical fluid phase values to typical gel phase values are indicators of a phase transition. Complementing the area per head group we determined the deuterium order parameter S_{CD}. The order parameter is a measure of the spatial restriction of the motion of the C−H vector[36] and is proportional to the deuterium quadrupolar splittings[37] in NMR measurements. The C−D bond order parameter for axially symmetric spectra is proportional to $S_{CC} = {}^1/_2\langle 3\cos^2\theta - 1\rangle$, where θ is the angle between the $C_{n-1}-C_n$ bond and the bilayer normal. We are approximating this by using the tailbeads (TB), i.e., we measure S_{TB-TB}. This quantity cannot be measured directly in experiments; however, there is a recurrent formulation that allows calculating S_{CC} from S_{CD} order parameters. For the C_n groups the direction is taken as z, and the deuterium order parameter for the nth carbon in computer simulations can be calculated by

$$-S_{CD}^n = \frac{2}{3}S_{xx}^n + \frac{1}{3}S_{yy}^n$$

Here $S_{JJ} = \langle \cos\theta_j \cos\theta_j - \delta_{jj}\rangle$ and $j = x, y, z$ with $\cos\theta_j = \hat{u}_j \hat{u}_z$. $\hat{u}_j$ is the unit vector for the j molecular axis in the bilayer, and $\hat{u}_z$ is the unit vector in the z direction. We calculated order parameters for the interaction centers of the tails TB_n that are neighbored by TB_{n-1} and TB_{n+1}. In the case of DLPC order parameters were calculated for one group and in the case of DSPC for three groups. These values provide another means for quantitative comparisons between experiments and simulations since they are accessible through NMR measurements.[38] Lipid order parameters depend on the temperature and the

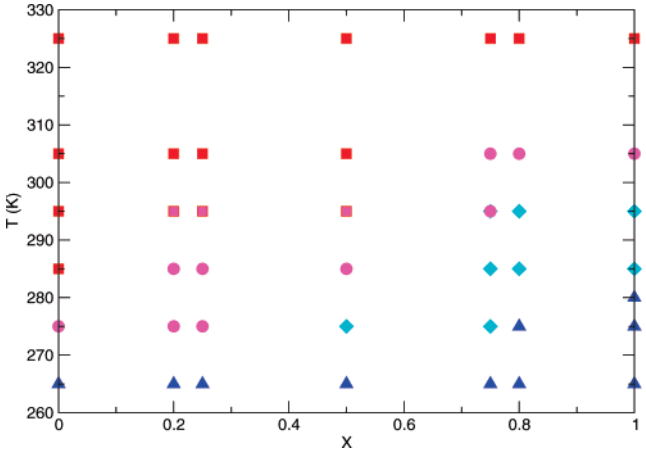

Figure 4. Schematic representation of order parameters for the TB_2 group of DSPC as a function of temperature and DSPC composition for a whole range of DLPC:DSPC concentrations. Red squares represent TB order parameters lower than 0.29, pink circles values between 0.29 and 0.32, cyan diamonds values between 0.33 and 0.42, and blue triangles values above 0.43.

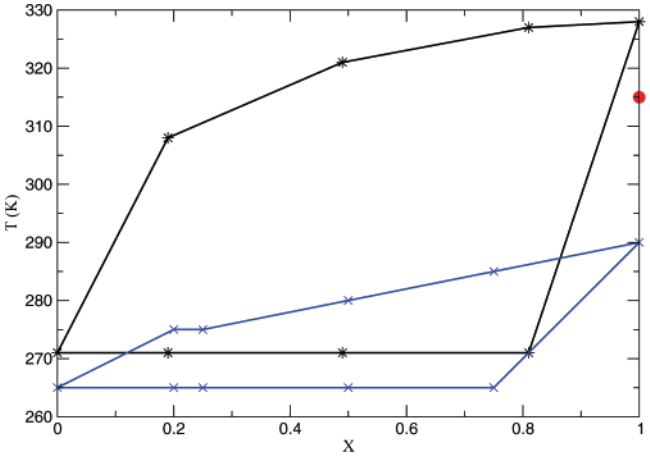

Figure 5. Phase diagram of temperature vs DSPC composition obtained with coarse-grained molecular dynamics simulations: the experimental phase diagram (black),[18] the simulated phase diagram obtained with cooling cycles (blue), and points for heating cycles (red) showing the strong hysteresis of the system.

position along the acyl chain. Typical values for the gel phase[39] are on the order of 0.4 and for the liquid crystalline[34,40] phase values are in the order of 0.02−0.3. We observe a flexibility gradient along the chain, and a slight difference in order between the two chains; however, we always took the average value for each group in the two chains. The S_{n-1} chain is slightly more ordered than S_{n-2} (data not shown); these observations correlate with the variation of quadrupolar splitting with chain position as reported for DPPC in the liquid crystalline phase.[37]

In Figure 4 we show a schematic representation of the order parameters for the TB_2 group in DSPC at different temperatures and for the whole range of molar ratios. We assigned colors and shapes for regions of order parameter values: red squares for order parameters lower than 0.29, pink circles for order parameter values between 0.29 and 0.32, cyan diamonds for order parameters between 0.33 and 0.42, and blue triangles for values above 0.43. As stated above, the changes in order parameter as well as in the areas per head group from values corresponding to the typical fluid phase to values corresponding to the typical gel phase are indicators of a phase transition.

Construction of a temperature composition phase diagram for a lipid mixture with a molecular based model has its challenges in determining the temperature limits for liquid and gel phases. These temperatures depend strongly on the model used, the system size, the length of the simulation, and, as in experiments, on the hysteresis of the lipid systems,[17] the rate of cooling, the starting structure, and temperature, i.e., thermal history is relevant.[41] A comparison of the effect of simulation time and system size for this model has been reported.[8] Judging from that data we can be sure that the size of the systems and the simulation time we selected are adequate to give reliable values within the model, keeping in mind that predicted temperatures for this model differ 20 to 30 K from the respective experimental values. This gap decreases by increasing system size as well as simulation length. Marrink et al.[8] reported phase transition temperatures for DPPC differ by about 15−20 K when extrapolating to large systems bigger than 2000 lipids, and simulation runs larger than 10 μs.

Since liquid and gel transitions do not occur at the same temperature because of hysteresis effects, we tested for hysteresis by cooling down and heating up pure DSPC systems. The experimental value for the transition temperature (T_m) for DSPC is 329 K;[18] we found a phase transition under cooling (quenching) between 285 and 290 K, and under heating (inverse quenching) between 315 and 325 K. This means that for heating simulations the bilayer at 315 K is probably in a metastable gel phase in this model, so it remains a gel beyond the transition temperature. In the same way for cooling simulations, the bilayer at 290 K is probably in a supercooled fluid phase, i.e., the fluid phase remains stable beyond the transition temperature. After characterization of the hysteresis, we set a uniform reference for the calculation of T_m for all systems: we start with a configuration equilibrated at a high temperature of 385 K and then cooled down by quenching the bilayer to the desired temperature. Changes in the order parameter, area per head group, radial distribution functions, as well as rotational and lateral diffusion dynamics were taken as indicators of a phase transition. This leads to the phase diagram in Figure 5. Property estimates above the upper limit curve represent liquid crystalline values, and in the same way for the lower limit curve, order parameters, areas per head group, and diffusional and rotational behavior are characteristics of the ordered phase. The comparison of our data with the experimental phase diagram[18] shows our diagram follows the shape of the experimental phase diagram, but it is displaced in temperature and only shows a narrow region of phase separation. This semiquantitative description is due mainly to the nature of the coarse-grained model; nevertheless the model reproduces the fundamental phase diagram shape. We already mentioned that larger systems and simulation times will give more accurate values. Heating cycle data for DSPC are shown in red and illustrate the strong hysteresis (cf. Figure 5).

Once the phase diagram was mapped out, we tested if we find phase coexistence between the liquid and the gel phase. For that we evaluated the dynamical heterogeneities in the suggested coexistence region. This is performed by analysis of the reorientation correlation function of the first Legendre polynomial $C_1(t) = \langle \vec{u}(t)\vec{u}(0)\rangle$, where $\vec{u}(t)$ and $\vec{u}(0)$ are unit vectors at time 0 and time t. The reorientation correlation function can be applied to characterize the tail dynamics of the lipids by monitoring the reorientation of the vector connecting the TB_1-TB_1 interaction sites of each tail (cf. Figure 1). At the phase transition it was observed that the tail dynamics decouples from the head dynamics, which corresponds to fast tail decay for lipids in the liquid crystalline phase and slow tail decay for lipids in the gel phase, for which there is a decrease in the rotational correlation time.[8] Experiments reported[37] that DPPC

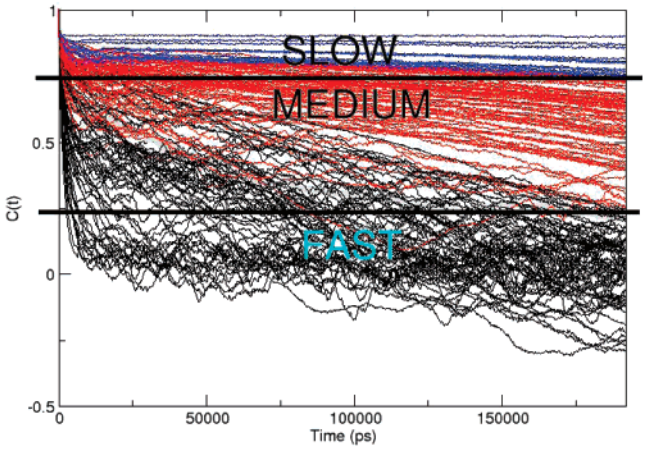

Figure 6. Rotational correlation function for 150 randomly chosen individual lipid molecules of DLPC at 270 K in a mixture of 4 times DLPC with respect to DSPC. The reorientation functions in blue are slow, red medium, and black fast.

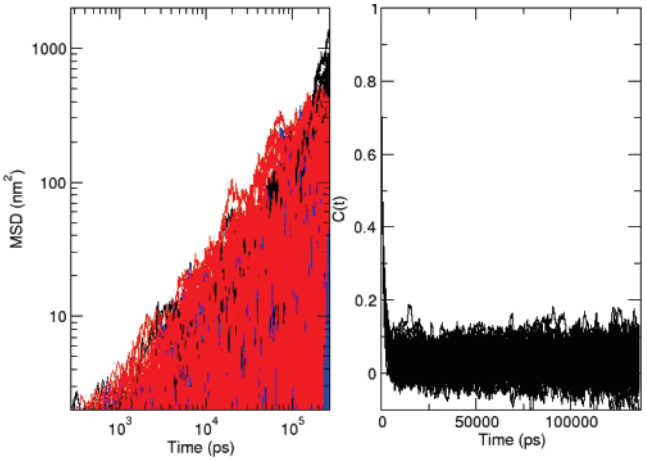

Figure 7. Mean square displacement (left) and rotational correlation function (right) for individual DSPC lipids in the liquid crystalline phase. The overall values of MSD and rotational function are calculated by the average of the individual values. We show 100 individual functions each—the same randomly selected lipids are shown on both sides. For the reorientation correlation function we see a clear difference to Figure 6, i.e., here all lipids reorient homogeneously fast but the mean square displacements are heterogeneous. The color code is the following: black fast, red medium, and blue slow. We designate a lipid as fast if its MSD at 270 ns is >500 nm^2 and slow if it is less than 50 nm^2.

in the gel phase undergoes axially symmetric reorientation on time scales of 2×10^{-5} s. It is important to note that the rotational diffusion for the whole lipid molecule is negligible on time scales of 10^{-8} to 10^{-10} s, where only a torsional rotation motion of the individual lipid chains is allowed.[27] In Figure 6 we see the reorientation functions for every DLPC lipid molecule in a 4DLPC:1DSPC molar ratio mixture of 57 648 atoms at 270 K and we find that the reorientation functions for each vector TB_1-TB_1 can be categorized in fast, medium, and slow or no reorientation of the lipid tails. This is an indicator of the existence of dynamic heterogeneity within DLPC; similar behavior was also observed for DSPC. To define in the lipid mixture which lipid populations have fast, medium, and slow orientation of the tails, we arbitrary selected values of the rotational correlation. Lipid molecules with values of $C(t)$ between 0 and 0.25 were considered fast, lipid molecules with values of $C(t)$ between 0.25 and 0.75 were considered medium, and lipid molecules with values of $C(t)$ between 0.75 and 1 were considered slow. The analysis of the rotational correlation functions for the lipids gives lipid populations that presented characteristics of fluid and gel states. From that, we got that 97% of the fast lipids are DLPC, 85% of the medium lipids are DLPC, and 85% of the slow lipids are DSPC. This is a clear indication that the system phase separates. However, these systems are small compared to experimental systems. Macroscopic phase separation would lead to domains much larger than these computational systems. We are limited to cluster sizes on the order of a few nanometers. A similar study of patterned bilayers[22] shows that the domain shapes are also influencing the phase behavior. Larger bilayer simulations over longer simulation times would probably favor the fluid phase and move the phase boundary because of increasing undulations.

It is important to note that the definition of dynamical heterogeneity depends on the type of motion. In Figure 7, we show both rotational and lateral diffusion motions for a bilayer in the liquid crystalline phase. We see for the rotational correlation function of each individual lipid (Figure 7, right) that the dynamic heterogeneity disappears, and the bilayer contains only fast lipids with rotation correlation times in the order of nanoseconds. It is known that for rotational motion relaxation times for gel phase lipids are larger[37] than the microsecond time scale allowing the identification of dynamic heterogeneities more evident in the case of coexisting fluid and gel phases. On the other side, for the lateral diffusion motion in Figure 7 (left) we have a distribution of mean square displacement for each individual lipid molecule in the bilayer, which defines the dynamic heterogeneity for this particular motion. For the gel and liquid crystalline phase we expect such a distribution of individual mean square displacements, with average diffusion coefficients differing by approximately 2 orders of magnitude between phases. So heterogeneities which are evident in the analysis of lateral diffusion cannot be used to characterize phase states. However, for microsecond time scales identification of dynamics heterogeneities using rotational correlations is more evident since relaxation times are larger.

3.3. Size Effects, Leaflet Composition, and Macroscopic versus Mesoscopic Phase Separation. For larger systems sizes undulations of the bilayer become important. This stabilizes the liquid crystalline phase, and the transition temperature (T_m) rises. In smaller systems the gel phase is more stabilized, so calculation of T_m depends both on system size and simulation time. For instance, we estimated the corresponding temperature for the upper curve of the phase diagram for a 512 lipid system to be 280 K, so at 275 K the system presented dynamic heterogeneity. Larger systems of 2048 lipids at 275 K show a dynamic heterogeneity with a higher proportion of lipids in the liquid crystalline state. We performed some additional simulations using unequal concentrations in the leaflets as cell membranes do not have balanced concentrations. The composition in the leaflets changes the phase transition temperature T_m. Thus, we may have phase coexistence in one leaflet and not in the other. This effect is negligible when the overall imbalance defined as the number of lipids differing in both leaflets is less than 3%. In addition it is important to consider the local imbalance for each type of lipid in the mixture, since larger amounts of one lipid kind in a leaflet compared to the other leaflet drive different phase states for each leaflet and incorrect calculations of the area per head group. For example, we performed simulations for two bilayers presenting the same system size of 256 DLPC and 64 DSPC lipids, but differing in lipid composition in both leaflets. The first bilayer has the same composition of DLPC and DSPC in both leaflets. The second bilayer has different composition and an overall imbalance of

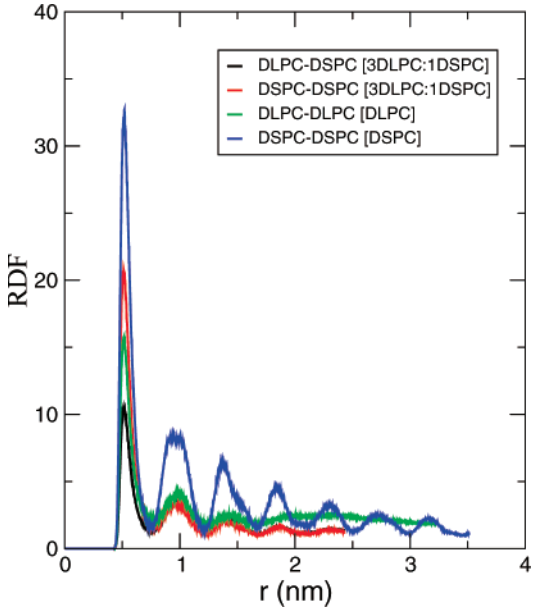

Figure 8. Radial distribution functions of TB_1-TB_1 centers of DLPC and DSPC at 275 K for the 3 to 1 molar ratio of DLPC with respect to DSPC. Pure DLPC and DSPC are included.

9%; comparison of the different T_m for both bilayers gave transition temperatures shifted by 10 K.

The transition temperature (T_m) of lipid bilayers can also be estimated by preconstructing bilayers with patches of fluid DLPC and gel DSPC with sizes within the matrix to test at what temperature these patterns grow into a gel phase state or liquid crystalline state, and at what temperatures there is phase coexistence. We also performed these types of simulations,[22] and found that for higher concentrations of DLPC than DSPC most bilayers freeze at 275 K, and their patterns are dissolved at 295 K, so again there is a small region of fluid and gel phase coexistence that depends on the pattern type in the bilayer and is displaced to higher temperatures with respect to the region determined for the outlined phase diagram that presents mesoscopic phase separation in contrast to macroscopic phase separation.

3.4. Mixing Behavior. We characterized mixtures of DLPC and DSPC at different concentrations and temperatures. As the concentration of DSPC, the more ordered lipid, increases, the lipid mixtures adopt a more ordered state. The mixing and order can be captured by radial distribution functions (RDF) of the TB_1 groups of the tails in order to avoid spurious effects of head group tilt. The RDF in Figure 8 shows for pure DSPC at 275 K long range order. The lack of order for pure DLPC indicates a fluid phase. Mixtures of DLPC−DSPC have an intermediate behavior. We observe that DSPC has a preference of neighbors of DSPC suggesting nonideal mixing; this observation is in agreement with experimental evidence.[34,40,42] It also correlates with the area per head group and order parameter data. We measure the area per lipid at constant temperature for the mixtures; we obtain at 275 K 0.46 nm^2 for 4:1 DSPC:DLPC, 0.48 nm^2 for 3:1, and 0.57 nm^2 for both 1:3 and 1:4. This indicates that the lipid with the highest concentration in the mixture dominates the values of the area per lipid. The order parameter of the tails also follows the same behavior. These are indicators of the nonlinear dependence of the properties on composition.

For the evaluation of the diffusion coefficient we use the Einstein relation, where the mean square displacement (MSD) for lateral diffusion is related to the self-diffusion constant D

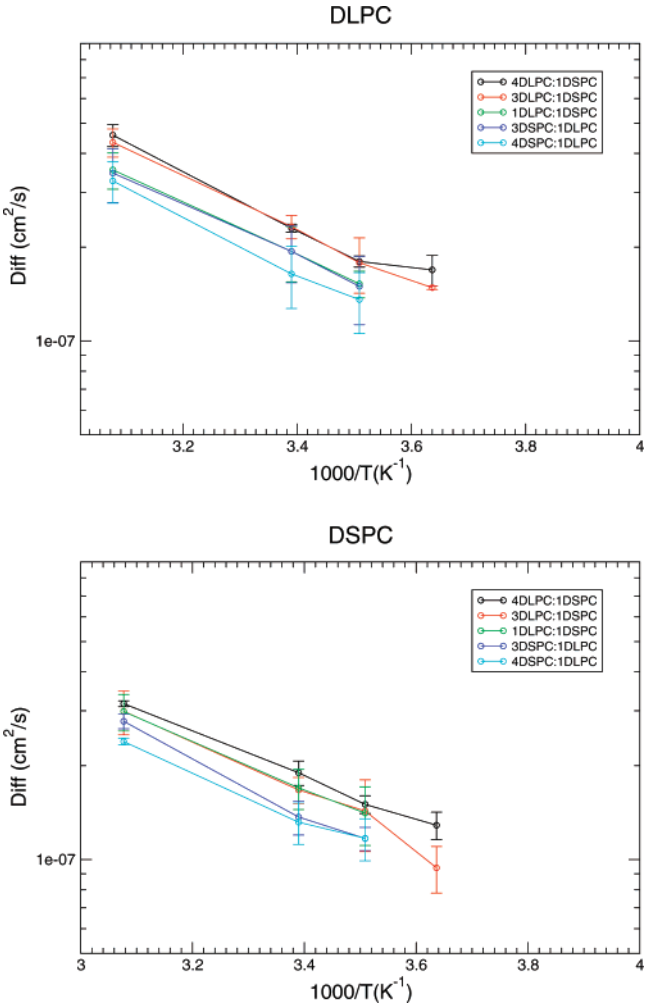

Figure 9. Arrhenius plot of the diffusion coefficients versus temperature for DLPC:DSPC lipid mixtures. Error bars were obtained by dividing the run into intervals of 1600 and 1200 ns.

TABLE 2: Activation Energies for Diffusion in DLPC:DSPC Lipid Mixtures

composition	E_a(DLPC) (kJ/mol)	E_a(DSPC) (kJ/mol)
4DSPC:1DL PC	17.16	17.94
3DSPC:1DLPC	15.97	17.10
1DSPC:1DLPC	15.96	15.25
3DLPC:1DSPC	15.98	17.12
4DLPC:1DSPC	15.55	13.59

by $D_{lat} = \lim_{t\to\infty} {}^1/_4\langle|r_i(t) - r_i(0)|^2\rangle$ assuming time intervals sufficiently long for it to be considered a linear regime. MSD is defined as $\langle r^2(t)\rangle = 1/N\sum_i\langle|r_i(t) - r_i(0)|^2\rangle$, with $r_i(t) - r_i(0)$ the vector distance traveled by molecule i over time t, so MSD represents an average over many such time intervals and over all molecules. The diffusion coefficients for all mixtures were evaluated at the microsecond time scale. At these time scales lipids diffuse beyond their neighbors allowing observation of truly diffusive behavior in contrast with nanosecond time scales in atomistic simulations. For the diffusion coefficient calculations, we performed statistical evaluation of the results with error analysis in the following way: mean square displacements were obtained for three different sets between 400 and 2000 ns; between 1200 and 2800 ns; and between 2800 and 4000 ns. The diffusion coefficients in Figure 9 represent the average values with their respective standard deviation. We used linear regression to calculate the diffusion coefficients in the liquid crystalline phase, yielding values of the lateral diffusion

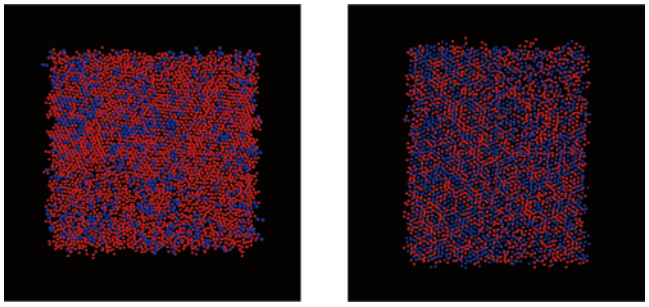

Figure 10. Snapshots for the TB_1 centers of DLPC (red) and DSPC (blue). From left to right we have the 2048:512 DLPC:DSPC mixture and an equimolar mixture of 1024:1024 DLPC:DSPC.

coefficient on the order of 10^{-7}cm^2/s with larger values corresponding to bilayers with more DLPC and lower values corresponding to bilayers more concentrated in DSPC (cf. Figure 9). Values for fluid phase lipid membranes with NMR and fluorescent microscopy[42] techniques, which are sensitive to larger time scales than the picoseconds time scales for neutron scattering, are in the order of 10^{-7} to 10^{-8} cm^2 per second;[16] bilayers of DPPC at 333 K present a diffusion coefficient of 10^{-7}cm^2/s.[27] All the diffusion coefficients reported in Figure 9 were obtained for the whole lipid molecules. The activation energies (E_a) for diffusion in lipid mixtures of DLPC and DSPC were also calculated by $\ln(D) = \ln(D_0) - E_a/RT$ and are shown in Table 2. This formulation considers the energy factor in the diffusion coefficient in agreement with the generalized free-area lipid diffusion models,[43] where the lipid diffusion increases with the probability of finding a free area and D and D_0 are the respective diffusion coefficients with and without hindrance. Activation energies are a function of the lipid interactions as well as the energy required to create a hole next to the diffusing molecule. DSPC has a larger diffusion activation energy than DLPC by about 17%. The errors, however, are on the same order of magnitude. The diffusion movements are slowed at higher concentrations of DSPC in the mixtures, since microscopic interactions and conformations for DSPC are stronger than for DLPC.

In Figure 10, we present snapshots at the coexistence region for a lipid mixture with higher concentration of DLPC (left) and for the equimolar case (right). The lipid mixture with a higher concentration of DSPC was shown elsewhere.[9] For systems with a higher concentration of DLPC, the clusters of DSPC are smaller than those for the equimolar mixture. The nonideal mixing behavior was also corroborated with radial distribution functions (Figure 8) and is present over the whole range of concentrations. For mixtures with a higher concentration of DSPC with respect to DLPC,[9] fluid clusters of DLPC with few DSPC are surrounded by gel phase DSPC; the inverse situation is depicted in Figure 10. In the liquid crystalline phase some extent of demixing was observed, with lipids of the same type preferring each other; this may lead to the existence of two liquid phases: higher demixing is observed at temperatures closer to T_m, and it decrease as T increases.

3.5. Phase Transformation. The phase transformation from liquid to gel phase can be followed over time by quenching the system instantaneously from $T > T_m$ to $T < T_m$. The phase transformation we observed is from L_α to $L_{\beta'}$; this gel phase does not present tilt in the tails as reported for pure DPPC.[8] The nature of this phase was characterized by changes in the dynamical properties over 2 orders of magnitude.[8] Another important observation is that the phase transformation is mainly driven by the lipid tails, since in the gel phase lipid head groups still have large rotational motion (defined by the PO4−CN3 vector reorientation) in the order of nanoseconds with respect to the tails, which are in the order of microseconds after extrapolation of the reorientation time.[8,9,37] In Figure 11 we show several snapshots at different times for a bilayer with equimolar concentration of DLPC and DSPC. At time zero, we have a bilayer that has been equilibrated well above the transition temperature; the system is in a liquid crystalline phase and presents some extent of demixing. As time progresses several clusters of more highly ordered lipids appear, and disappear again as they are unstable. Around 80 ns a larger size stable cluster (i.e., a critical nucleus) has formed and grows driving the system to a gel state. This is indicative of a nucleation and growth scenario. These observations suggest that the fluid−gel phase transformation has as critical step, the nucleation of a stable gel cluster. Finally we observe a bilayer with a higher order phase. The RDF for this structure in Figure 12 shows a nonideal mixing behavior in the gel state with a long range ordering, where DSPC lipids prefer to be surrounded by DSPC lipids over DLPC; this clustering of DSPC is indicating the

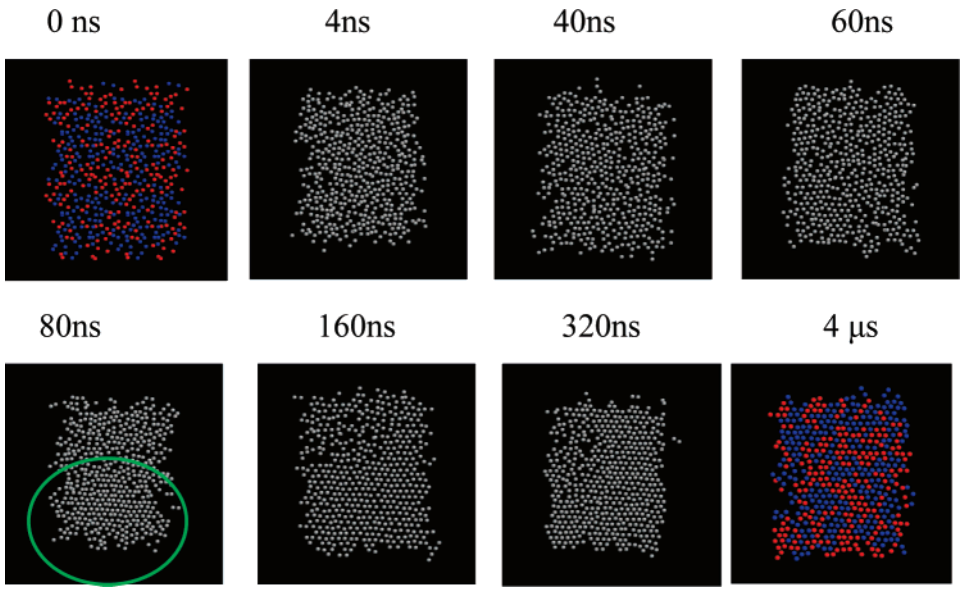

Figure 11. Fluid to gel phase transformation for the 256:256 mixtures. In the first and last snapshot DLPC is in red and DSPC in blue; the figures represent the TB_1 bead lattice.

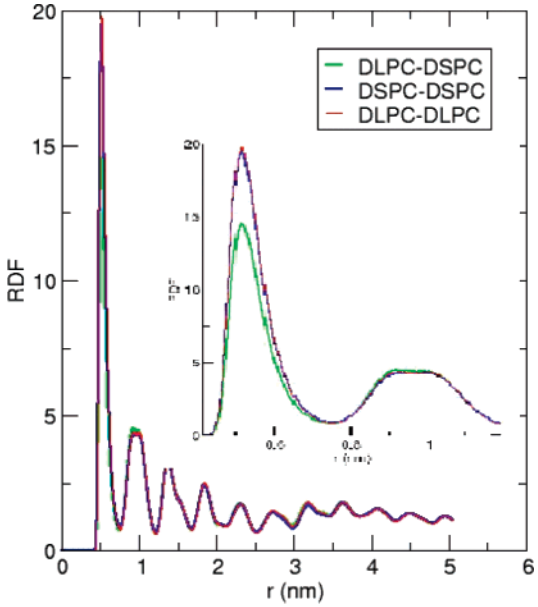

Figure 12. Radial distribution function of the TB_1 centers of the lipid chains indicating the nonideal behavior in the gel phase by showing the preference of DSPC and DLPC to be surrounded by the same type of lipid. The inset is a zoom on the small distance region.

nonideal mixing behavior that has been reported earlier,[18,19] when different chain length lipids are components of a lipid mixture.

4. Conclusions

We describe a series of molecular dynamic simulations in order to identify and quantify the molecular interactions in binary mixtures of phospholipid bilayers of DLPC:DSPC.

Understanding interactions of two component lipid mixtures is relevant for interpreting the possible interactions of complex lipid mixtures in biological membranes. Simulations were extended in system size and time compared to currently available atomistic simulations, and lipids still maintained their molecular characteristics.

The mixing behavior at the molecular level shows that properties of the mixtures do not change linearly with composition; we see demixing in the ideal fluid phase with a nonideal gel phase, where lipids of the same type prefer to cluster. The properties of the mixtures compare favorably with experimental data.

We determined static and dynamic properties to define variations in lipid structure from the liquid crystalline to gel phase. These variations in structure define a narrow region where we find a heterogeneous dynamics in the lipids, which allows us to outline the phase diagram, and we show that it roughly follows the shape of the experimental phase diagram for DLPC−DSPC. This shape represents a nonideal system and is mainly attributed to the large hydrophobic mismatch resulting from the difference in length between DLPC and DSPC. However, we have to stress that the determination of the limiting values of the phase diagram depends on the system size, simulation time, and thermal history. For our system sizes we find strong hysteresis; this even applies to coarse-grained water alone.

We conclude that molecular simulation can estimate the lower and upper limits of the phase coexistence profile, and within these limits dynamical heterogeneity is found. However, macroscopic phase separation could not be observed due to size limitations. We find mesoscopic phase separation or cooperative fluctuations; nevertheless, it is remarkable how the trend of the experimental phase diagram is followed by the simulations. It is noteworthy to mention that recently Murtola et al. have studied heterogeneities in different lipid bilayer systems as well.[44,45] They focused on the transient appearance and dissolution of domains and reported clustering effects similar to the ones reported here. In simulations it is always difficult to distinguish if the results are only a long-lived transient or true thermodynamic phase behavior. But taking all these studies together with the present one it clearly appears that there is a general consensus using widely different models to obtain at least mesoscale dynamical and thermodynamical fluctuations in phospholipid bilayers which may be relevant for the biological function of membranes.

We also discuss an alternative method for determination of the lower and upper limits of the melting profile: we patterned bilayers with fluid DLPC and gel DSPC, these bilayers indeed present domain sizes in the order of the matrix size,[22] reflecting macroscopic phase separations. For these patterned bilayers we see that the region of coexistence is displaced to higher temperatures with respect to the phase diagram outlined here, but still we see a short narrow region where fluid and gel phase coexist with estimated transition temperatures in semiquantitative agreement with the experimental values. These studies contribute to the understanding of lipid phase behavior with the advantage that a molecular based model allows following phase transformations and mixing behavior over the time and at the molecular level. In particular phase separation is of high interest, since it provides the possibility of studying domain nucleation and patterning from the theoretical side.[22,23]

Acknowledgment. This investigation was supported by the Graduate Research and Education in Adaptive bio-Technology (GREAT) Training Program of the UC Systemwide Biotechnology Research and Education Program under grant no. 2005-244. We also acknowledge computer time at the National Center for Supercomputing Applications (NCSA), and the San Diego Supercomputer Center (SDSC) (Project Nos. MCB050018N and TG-MCB050071T). The NSF MRSEC Center for Polymer Interfaces and Macromolecular Assemblies, and the NSF NIRT (grant no. CBET 0506602) Program supported this research as well.

References and Notes

(1) Simons, K.; Ikonen, E. *Nature* **1997**, *387*, 569.
(2) Brown, D. A.; London, E. *Annu. Rev. Cell Dev. Biol.* **1998**, *14*, 111.
(3) Varma, R.; Mayor, S. *Nature* **1998**, *394*, 798.
(4) Brown, D. A.; London, E. *J. Biol. Chem.* **2000**, *275*, 17221.
(5) De Angelis, D. A.; Miesenbock, G.; Zemelman, B. V.; Rothman, J. E. *Proc. Natl. Acad. Sci. U.S.A.* **1998**, *95*, 12312.
(6) Sheets, E. D.; Lee, G. M.; Simson, R.; Jacobson, K. *Biochemistry* **1997**, *36*, 12449.
(7) Kraft, M. L.; Weber, P. K.; Longo, M. L.; Hutcheon, I. D.; Boxer, S. G. *Science* **2006**, *313*, 1948.
(8) Marrink, S. J.; Risselada, J.; Mark, A. E. *Chem. Phys. Lipids* **2005**, *135*, 223.
(9) Faller, R.; Marrink, S. J. *Langmuir* **2004**, *20*, 7686.
(10) Stevens, M. J. *J. Am. Chem. Soc.* **2005**, *127*, 15330.
(11) London, E. *Biochim. Biophys. Acta*- **2005**, *1746*, 203.
(12) Smart, E. J.; Graf, G. A.; McNiven, M. A.; Sessa, W. C.; Engelman, J. A.; Scherer, P. E.; Okamoto, T.; Lisanti, M. P. *Mol. Cell. Biol.* **1999**, *19*, 7289.
(13) Gousset, K.; Wolkers, W. F.; Tsvetkova, N. M.; Oliver, A. E.; Field, C. L.; Walker, N. J.; Crowe, J. H.; Tablin, F. *J. Cell. Physiol.* **2002**, *190*, 117.
(14) de Almeida, R. F.; Loura, L. M.; Fedorov, A.; Prieto, M. *Biophys. J.* **2002**, *82*, 823.
(15) Jorgensen, K.; Klinger, A.; Biltonen, R. L. *J. Phys. Chem. B* **2000**, *104*, 11763.

(16) Hac, A. E.; Seeger, H. M.; Fidorra, M.; Heimburg, T. *Biophys. J.* **2005**, *88*, 317.
(17) Ricker, J. V.; Tsvetkova, N. M.; Wolkers, W. F.; Leidy, C.; Tablin, F.; Longo, M.; Crowe, J. H. *Biophys. J.* **2003**, *84*, 3045.
(18) Mabrey, S.; Sturtevant, J. M. *Proc. Natl. Acad. Sci. U.S.A.* **1976**, *73*, 3862.
(19) Ipsen, J. H.; Mouritsen, O. G. *Biochim. Biophys. Acta* **1988**, *944*, 121.
(20) Elliott, R.; Katsov, K.; Schick, M.; Szleifer, I. *J. Chem. Phys.* **2005**, *122*.
(21) Sugar, I. P.; Thompson, T. E.; Biltonen, R. L. *Biophys. J.* **1999**, *76*, 2099.
(22) Bennun, S. V.; Longo, M.; Faller R. Submitted for publication.
(23) Switzer, J. M.; Bennun, S. V.; Longo, M. L.; Palazoglu, A.; Faller, R. *J. Chem. Phys.* **2006**, *124*, 234906.
(24) Marrink, S. J.; de Vries, A. H.; Mark, A. E. *J. Phys. Chem. B* **2004**, *108*, 750.
(25) Marrink, S. J.; Mark, A. E. *J. Am. Chem. Soc.* **2003**, *125*, 15233.
(26) Marrink, S. J.; Mark, A. E. *Biophys. J.* **2004**, *87*, 3894.
(27) Sackmann, E. *Handbook of Biological Physics*; Elsevier Science: Amsterdam, The Netherlands, 1995; Vol. I.
(28) Jacobs, R. E.; Hudson, B. S.; Andersen, H. C. *Biochemistry* **1977**, *16*, 4349.
(29) Wong, B. Y.; Faller R. *Biochim. Biophys. Acta* **2007**, *1768* (3), 620.
(30) Van der Spoel, D.; Lindahl, E.; Hess, B.; Groenhof, G.; Mark, A. E.; Berendsen, H. J. C. *J. Comput. Chem.* **2005**, *26*, 1701.
(31) Berendsen, H. J. C.; Postma, J. P. M.; Vangunsteren, W. F.; Dinola, A.; Haak, J. R. *J. Chem. Phys.* **1984**, *81*, 3684.
(32) Bennun, S.; Dickey, A. N.; Xing, C.; Faller, R. *Simulations of Biomembrane and Water*: *Important Technical Aspects*. Submitted for publication.
(33) Balgavy, P.; Dubnickova, M.; Kucerka, N.; Kiselev, M. A.; Yaradaikin, S. P.; Uhrikova, D. *Biochim. Biophys. Acta* **2001**, *1512*, 40.
(34) Petrache, H. I.; Dodd, S. W.; Brown, M. F. *Biophys. J.* **2000**, *79*, 3172.
(35) Balgavy, P.; Dubnickova, M.; Kucerka, N.; Kiselev, M. A.; Yaradaikin, S. P.; Uhrikova, D. *Biochim. Biophys. Acta* **2001**, *1512*, 40.
(36) Tieleman, D. P.; Marrink, S. J.; Berendsen, H. J. C. *Biochim. Biophys. Acta* **1997**, *1331*, 235.
(37) Davis, J. H. *Biochim. Biophys. Acta* **1983**, *737*, 117.
(38) Koenig, B. W.; Strey, H. H.; Gawrisch, K. *Biophys. J.* **1997**, *73*, 1954.
(39) Bolterauer, C.; Heller, H. *Eur. Biophys. J. Biophys. Lett.* **1996**, *24*, 322.
(40) Petrache, H. I.; Tu, K. C.; Nagle, J. F. *Biophys. J.* **1999**, *76*, 2479.
(41) Lin, W. C.; Blanchette, C. D.; Ratto, T. V.; Longo, M. L. *Biophys. J.* **2006**, *90*, 228.
(42) Ratto, T. V.; Longo, M. L. *Biophys. J.* **2002**, *83*, 3380.
(43) Macedo, P. B.; Litovitz, T. A. *J. Chem. Phys.* **1965**, *42*, 245.
(44) Murtola, T.; Róg, T.; Falck, E.; Karttunen, M.; Vattulainen, I. *Phys. Rev. Lett.* **2006**, *97*, 238102.
(45) Murtola, T.; Falck, E.; Karttunen, M.; Vattulainen, I. *J. Chem. Phys.* **2007**, *126*, 075101.